Alexandria Engineering Journal (2015) 54, 691–704

Alexandria University

Alexandria Engineering Journal

www.elsevier.com/locate/aej
www.sciencedirect.com

ORIGINAL ARTICLE

Peristaltic transport of MHD flow and heat transfer in an asymmetric channel: Effects of variable viscosity, velocity-slip and temperature jump

A. Sinha *, **G.C. Shit, N.K. Ranjit**

Department of Mathematics, Jadavpur University, Kolkata 700032, India

Received 30 July 2014; revised 22 March 2015; accepted 31 March 2015
Available online 8 May 2015

KEYWORDS

Peristaltic transport;
Heat transfer;
Variable viscosity;
Slip effects

Abstract In this article, a theoretical study is presented for peristaltic flow of a MHD fluid in an asymmetric channel. Effects of viscosity variation, velocity-slip as well as thermal-slip have been duly taken care of in the present study. The energy equation is formulated by including a heat source term which simulates either absorption or generation. The governing equations of motion and energy are simplified using long wave length and low Reynolds number approximation. The coupled non-linear differential equations are solved analytically by means of the perturbation method for small values of Reynolds model viscosity parameter. The salient features of pumping and trapping are discussed with particular focus on the effects of velocity-slip parameter, Grashof number and magnetic parameter. The study reveals that the velocity at the central region diminishes with increasing values of the velocity-slip parameter. The size of trapped bolus decreases and finally vanishes for large values of magnetic parameter.

1. Introduction

Peristaltic transport of physiological fluids induced by a progressive wave of area contraction or expansion along the length of a distensible tube has drawn serious attention of researchers working in the area of physiological fluid dynamics. To be more specific, it encounters in urine transport from the kidney to the bladder, through the ureter, chyme transport in the gastrointestinal tract, swallowing food through the esophagus, transport of spermatozoa in the ductus efferentes of the male reproductive tracts, the movement of the ovum in the female fallopian tube, and the vasomotion of small blood vessels. Also, finger and roller pumps are frequently used for pumps corrosive or very pure materials so as to prevent direct contact of the fluid with the pump's internal surfaces.

To understand the peristaltic action under different normal and pathological conditions, several theoretical and experimental attempts [1,2] have been made since the first investigation of Latham [3]. Aarts and Ooms [4] have developed a theory for peristaltic pumping of a compressible fluid in a

* Corresponding author.
E-mail address: aniruddha.sinha07@gmail.com (A. Sinha).
Peer review under responsibility of Faculty of Engineering, Alexandria University.

http://dx.doi.org/10.1016/j.aej.2015.03.030

Nomenclature

(X', Y')	Cartesian coordinates
(U', V')	velocity components along X' and Y' directions
c	wave speed
p'	fluid pressure
g	acceleration due to gravity
B_0	applied magnetic field strength
C_p	specific heat at constant pressure
Q_0	constant heat addition/absorption
Re	Reynolds number
M	Hartman number
P_r	Prandtl number
Gr	Grashof number
T_1	temperature of the upper wall
T_0	temperature of the lower wall

Greek symbols

λ	wave length
ϕ'	phase difference
μ'	variable viscosity
σ	electrical conductivity
ρ	density of blood
α_1	co-efficient of thermal expansion
κ	thermal conductivity
θ'	non-dimensional mean flow rate
θ	non-dimensional temperature
δ	wave number
β	heat source/sink parameter
β_1	velocity slip parameter
γ	thermal slip parameter
α	Reynolds model viscosity parameter

circular tube with a view to enhance oil production from porous rock by the application of ultrasound. Vries et al. [5] observed that due to myometrial contractions, the intrauterine fluid flow exhibits peristalsis and myometrial contractions may occur in both symmetric and asymmetric directions. Taylor [6] conducted a theoretical investigation on asymmetric wave propagation in wavy sheets with the main objective of deriving some information regarding the mechanical interaction between spermatozoa. Carew and Pedley [7] studied the pumping phenomenon of peristaltic flow in the ureter by using lubrication theory. By taking into account the wall deformation of the pipe, Antanovskii and Ramkissoon [8] have used lubrication theory in order to analyze the peristaltic transport of a compressible viscous fluid through a pipe for situations where the pressure drop changes with time. Nadeem and Akram [9] theoretically studied a peristaltic flow of a Williamson model in an asymmetric channel. Maiti and Misra [10] have investigated the peristaltic transport of bile flow within ducts in a pathological state. They remarked that in the presence of gallstones, the critical pressure for reflux decreases as porosity increases. Very recently, Akbar and Butt [11] have studied on the non-Newtonian Casson fluid model accompanied in a horizontal tube.

In the above mentioned studies fluid viscosity is assumed to be constant. There are few attempts [12,13] in which the effects of variable viscosity in the peristaltic mechanisms have been considered. These studies considered the viscosity to be a function of space variable in the form of an exponential function. In a typical situation most of the fluids have temperature dependent viscosity and this property varies significantly when large temperature difference exists. Elshehawey and Gharsseldien [14] studied the effects of variable viscosity for peristaltic motion of an incompressible Newtonian fluid through a channel with three layers flow. Martin [15] analytically solved the problem of viscometric flows of Power-law fluids with variable viscosity.

The red blood cell (erythrocyte) is a major biomagnetic substance and therefore, it is quite possible that blood flow is influenced by the presence of magnetic field. The flow rate of blood is reduced due to either an increase in blood flow resistance or a decrease in blood pressure. The effect of an externally applied magnetic field on blood flow has been analyzed theoretically by treating blood as an electrically conducting fluid [16]. The major mechanism of the influence of a stationary magnetic field on blood viscosity is based on the interaction between the induced magnetic moment of the erythrocytes (RBC) and the external stationary magnetic field. The RBC has greater susceptibility along its long axis. So, it tends to orient its long axis for larger magnetic susceptibility along the external magnetic field.

The peristaltic transport of magnetohydrodynamic (MHD) flow of a fluid in a channel is of interest in connection with certain problems of the movement of conductive physiological fluids, e.g., the blood, blood pump machines and with the need for experimental as well as theoretical research on the operation of a peristaltic MHD compressor. Effect of a moving magnetic field on blood flow was investigated by Sud et al. [17], and they observed that the effect of suitable moving magnetic field accelerates the speed of blood. Akbar [18] theoretically investigated the influence of magnetic field on peristaltic transport of nano Eyring-Powell fluid in an asymmetric channel. Agrawal and Anwaruddin [19] developed a mathematical model of MHD flow of blood through an equally branched channel with flexible walls executing peristaltic waves using long wave length approximation method and observed, for the flow blood in arteries with arterial disease like arterial stenosis or arteriosclerosis, that the influence of magnetic field may be utilized as a blood pump in carrying out cardiac operations. The principle of magnetic field is successfully applied to Magnetic Resonance Imaging (MRI) when a patient undergoes in a hight static magnetic field. Abbasi et al. [20] developed a mathematical model on peristaltic transport of MHD fluid by considering variable viscosity. Moreover, the influence of magnetic field on peristaltic flow of a Casson fluid in an asymmetric channel was studied by Akbar [21] who has also investigated the characteristics of fluid flow in tabular harmonizes by considering long wave length and low Reynolds number approximations [22]. Akbar [23] has carried out the influence of magnetic field on flow and heat transfer of a carbon nanotube induced by peristaltic waves and observed that

with the increase of solid volume fraction of the nanoparticles and heat absorption parameter, the temperature profile increases significantly.

Lauga and Stone [24] experimentally investigated the effective slip length of the resulting flow as a function of the degrees of freedom describing the surface heterogeneities, namely the relative width of the no-slip and no-shear stress regions and their distribution along the pipe. They concluded that the experimental results which are consistent with a large number of distributed slip domains such as nano-size and micron-size nearly flat bubbles coating the solid surface. In addition they also suggested the possibility of a shear-dependent effective slip length. Hayat et al. [25] discussed the effect of slip velocity on peristaltic transport of an incompressible viscous fluid in an asymmetric channel through a porous medium. According to them for large values of slip parameter the size of trapped bolus decreases and symmetry disappears. Furthermore, Hayat et al. [26] have examined the slip effect on Carreau–Yasuda fluid in a curved channel wherein they reported that an increase in velocity slip parameters decreases the peristaltic and retrograde pumping regions. Many authors [27,28] suggested the presence of a red blood cell slip at the vessel wall. Misra and Kar [29] solved the problem of blood flow through a stenosed vessel by taking into consideration the slip velocity at the wall by using the momentum integral technique. Ebert and Sparrow [30] and Sparrow et al. [31] analyzed several flow problems under some pathological states. Wang [32] considered a problem involving partial slip by considering stagnation point flows. Abbasi et al. [33] also investigated the peristaltic transport of copper–water nanofluid in an inclined channel in the presence of mixed convection. They found that velocity slip parameter has a decreasing effect on the velocity near the center of channel while the temperature of nanofluid enhances in the presence of Grashof number as well as inclination of the channel. Later on Hayat et al. [34] also theoretically analyzed the slip and joule heating effects in mixed convection peristaltic transport of nanofluid with Soret and Dufour effects.

While flowing through the arterial tree, blood carries a large quantity of heat to different parts of the body. On the skin surface, the transfer of heat can take place by any of the four processes: radiation, evaporation, conduction and convection. It may further be mentioned that blood flow enhances when a man performs hard physical work and also when the body is exposed to excessive heat environment. In cases like these, blood circulation cannot remain normal. In order to take care of the increase in blood flow, the dimensions of the artery have to increase suitably. It is known that when the temperature of the surroundings exceeds 20 °C, heat transfer takes place from the surface of the skin by the process of evaporation through sweating and when the temperature is below 20 °C, the human body loses heat by conduction and radiation both. Blood flow with radiative heat transfer was discussed by Ogulu and Bestman [35] on the basis of a theoretical study. The study of heat transfer analysis is an important area in connection with peristaltic motion, which has industrial applications such as sanitary fluid transport, blood pumps in heart lungs machine and transport of corrosive fluids where the contact of fluid with the machinery parts is prohibited. There is only a limited amount of research available in the literature in which peristaltic phenomenon has discussed in the presence of heat transfer [36,37].

To the best of our knowledge, no attempt is available in the literature which deals with the problem of peristaltic transport of MHD flow of blood and heat transfer in an asymmetric capillary blood vessel with variable viscosity when no-slip condition is inadequate. The no-slip condition is inadequate when one considers fluids exhibiting macroscopic wall slip and that in general is governed by relation between the slip velocity and traction. Due to such fact in mind, the main purpose of the present investigation is to examine the peristalsis of a magnetohydrodynamic (MHD) fluid with variable viscosity, velocity-slip as well as thermal-slip conditions. To the authors' best knowledge, this problem has not been even studied for the hydrodynamic fluid. The flow analysis is developed in a wave frame of reference moving with the velocity of the wave. In Section 2, the problem is first modeled and the non-dimensional governing equations are formulated in wave frame. The non-dimensional governing equations under the long wavelength and low Reynolds number approximation and the corresponding boundary conditions are prescribed in Section 3. In Section 4, perturbation analysis has been discussed. Section 5 includes the exact solution of the problem. The results for the velocity, temperature, pressure rise, pressure gradient, wall shear stress and stream function have been discussed for various values of the problem parameters in Section 6. Finally, the main conclusions are summarized in Section 7. It is expected that the results presented here will serve as fairly good theoretical estimates of various prospective fluid mechanical flow governing parameters related to the peristaltic transport of blood.

2. Mathematical model and governing equations

We consider the peristaltic transport of an unsteady incompressible and electrically conducting fluid through an asymmetric two dimensional channel (cf. Fig. 1) of width $d_1 + d_2$. We choose a stationary frame of reference (X', Y') such that X' measured along the axis of the channel and Y' perpendicular to X'. Let (U', V') be the velocity components in the fixed frame of reference (X', Y'). Again, we consider the flow is induced by sinusoidal wave trains propagating with constant speed c along the channel walls. The geometry of the wall surface (cf. [38]) is assumed to be

$$h_1'(X', t') = d_1 + a_1 \cos\left[\frac{2\pi}{\lambda}(X' - ct')\right], \quad \text{upper wall} \tag{1}$$

$$h_2'(X', t') = -d_2 - a_2 \cos\left[\frac{2\pi}{\lambda}(X' - ct') + \phi'\right], \quad \text{lower wall} \tag{2}$$

in which a_1 and a_2 are amplitudes of the waves, λ is the wave length, t' is the time $\phi\,(0 \leqslant \phi \leqslant \pi)$ is the phase difference. It should be noted that $\phi = 0$ corresponds to a symmetric channel with waves out of phase and for $\phi = \pi$ the waves are in phase. A uniform magnetic field is applied normal to that of flow. In this analysis, it is assumed that magnetic Reynolds number is much less than unity so that the induced magnetic field is negligible in comparison with applied magnetic field.

The Soret effect, also called thermophoresis, is a phenomenon observed when a mixture of different type particles, is under the action of temperature gradient, and the responses of the particles are different. At $t' \leq 0$, the walls of the channel and the fluid are assumed to beat the same temperature, so that the Soret effect is negligibly small.

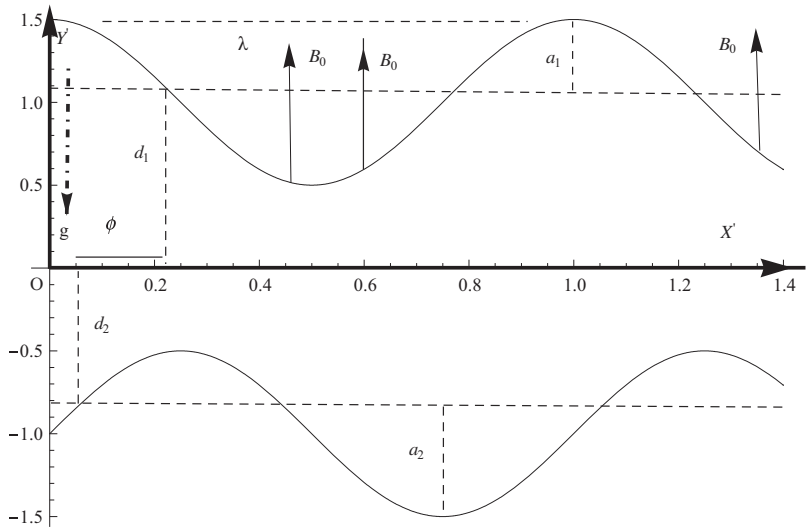

Fig. 1 A physical sketch of the problem.

With all the above mentioned consideration, the equations that govern the motion of the fluid in the wave frame may be listed as

$$\frac{\partial U'}{\partial X'}+\frac{\partial V'}{\partial Y'}=0, \tag{3}$$

$$\rho\left(\frac{\partial U'}{\partial t'}+U'\frac{\partial U'}{\partial X'}+V'\frac{\partial U'}{\partial Y'}\right)=-\frac{\partial P'}{\partial X'}+2\frac{\partial}{\partial X'}\left(\mu'(Y')\frac{\partial U'}{\partial X'}\right)+\frac{\partial}{\partial Y'}\left[\mu'(Y')\left(\frac{\partial V'}{\partial X'}+\frac{\partial U'}{\partial Y'}\right)\right]-\sigma B_0^2U'+\rho g\alpha_1(T'-T_0), \tag{4}$$

$$\rho\left(\frac{\partial V'}{\partial t'}+U'\frac{\partial V'}{\partial X'}+V'\frac{\partial V'}{\partial Y'}\right)=-\frac{\partial P'}{\partial Y'}+2\frac{\partial}{\partial Y'}\left(\mu'(Y')\frac{\partial V'}{\partial Y'}\right)+\frac{\partial}{\partial X'}\left[\mu'(Y')\left(\frac{\partial V'}{\partial X'}+\frac{\partial U'}{\partial Y'}\right)\right], \tag{5}$$

$$\rho C_p\left(\frac{\partial T'}{\partial t'}+U'\frac{\partial T'}{\partial X'}+V'\frac{\partial T'}{\partial Y'}\right)=\kappa\left[\frac{\partial^2T'}{\partial X'^2}+\frac{\partial^2T'}{\partial Y'^2}\right]+Q_0, \tag{6}$$

where the definition of all the symbols involved in the equations is included in the Nomenclature.

In the laboratory frame (X', Y') the flow is unsteady. However if observed in a co-ordinate system moving at the wave speed c in the wave frame (x', y'), it can be treated as steady. The co-ordinates, velocities, pressure and temperature in the two frames are

$$x'=X'-ct',\quad y'=Y',\quad u'=U'-c,\quad v'=V',\quad p'=P',\quad T=T', \tag{7}$$

where U', V' and u', v' are the velocity components in the corresponding co-ordinate systems. Let us introduce the following non-dimensional variables [38]:

$$x=\frac{x'}{\lambda},\ y=\frac{y'}{d_1},\ u=\frac{u'}{c},\ v=\frac{\lambda v'}{d_1c},\ p=\frac{d_1^2p'(x')}{\lambda\mu c},\ t=\frac{ct'}{\lambda},\quad \theta=\frac{T-T_0}{T_1-T_0},\ h_1(x)=\frac{h_1'(x')}{d_1},\ h_2(x)=\frac{h_2'(x')}{d_1},\ \mu(y)=\frac{\mu'(y')}{\mu_0} \tag{8}$$

in which μ_0 is the constant viscosity and δ is the wave number.

Invoking Eq. (8) into Eqs. (3)–(6) we have

$$\frac{\partial u}{\partial x}+\frac{\partial v}{\partial y}=0, \tag{9}$$

$$R_e\delta\left((u+1)\frac{\partial u}{\partial x}+v\frac{\partial u}{\partial y}\right)=-\frac{\partial p}{\partial x}+2\delta^2\frac{\partial}{\partial x}\left(\mu(y)\frac{\partial u}{\partial x}\right)+\frac{\partial}{\partial y}\left[\mu(y)\left(\delta^2\frac{\partial v}{\partial x}+\frac{\partial u}{\partial y}\right)\right]-M^2(u+1)+Gr\theta, \tag{10}$$

$$R_e\delta^3\left((u+1)\frac{\partial v}{\partial x}+v\frac{\partial v}{\partial y}\right)=-\frac{\partial p}{\partial y}+2\delta^2\frac{\partial}{\partial y}\left(\mu(y)\frac{\partial v}{\partial y}\right)+\frac{\partial}{\partial x}\left[\mu(y)\left(\delta^2\frac{\partial v}{\partial x}+\frac{\partial u}{\partial y}\right)\right], \tag{11}$$

$$\delta R_eP_r\left((u+1)\frac{\partial\theta}{\partial x}+v\frac{\partial\theta}{\partial y}\right)=\left[\delta^2\frac{\partial^2\theta}{\partial x^2}+\frac{\partial^2\theta}{\partial y^2}\right]+\beta, \tag{12}$$

where δ, R_e, M, Gr, P_r, β are non-dimensional parameters, called respectively the wave number, Reynolds number, Hartmann number, Grashof number, Prandtl number and source/sink parameter given by

$$\delta=\frac{d_1}{\lambda},\quad R_e=\frac{\rho d_1c}{\mu_0},\quad M=\sqrt{\frac{\rho}{\mu_0}}B_0d_1,\quad Gr=\frac{\rho g\alpha(T_1-T_0)d_1^2}{c\mu_0},\quad P_r=\frac{\mu_0c_p}{\kappa},\quad \beta=\frac{Q_0d_1^2}{\kappa(T_1-T_0)} \tag{13}$$

Introducing the stream function $u=\frac{\partial\psi}{\partial y}$, $v=-\frac{\partial\psi}{\partial x}$, in the Eqs. (9)–(12) and under the assumptions of long wave length ($\delta\ll1$) and low Reynolds number will take the form

$$0=-\frac{\partial p}{\partial x}+\frac{\partial}{\partial y}\left[\mu(y)\frac{\partial^2\psi}{\partial y^2}\right]-M^2\left(\frac{\partial\psi}{\partial y}+1\right)+Gr\theta, \tag{14}$$

$$0=-\frac{\partial p}{\partial y}, \tag{15}$$

$$0=\frac{\partial^2\theta}{\partial y^2}+\beta. \tag{16}$$

It is noted that from Eq. (15) that p is not a function of y.

3. Volumetric flow rate and boundary conditions

The instantaneous volume flow rate in fixed frame is given by

$$Q = \int_{h_2'}^{h_1'} U'(X', Y', t')dy', \tag{17}$$

where h_1' and h_2' are functions of X' and t'.

The volumetric flow rate in the wave frame is given by

$$q = \int_{h_2'}^{h_1'} u'(x', y')dy', \tag{18}$$

where h_1' and h_2' are functions of x' only.

If we substitute (7) into (17) and make use of (18), we find that the two rates of volume flow are related through

$$Q = q + c(h_1' - h_2'). \tag{19}$$

The time mean flow over a period T_2 $(= \frac{\lambda}{c})$ at a fixed position X' can be written as

$$Q' = \frac{1}{T_2}\int_0^{T_2} Q dt. \tag{20}$$

Substituting Eq. (19) into (20) and integrating, we arrive at

$$Q' = q + c(d_1 + d_2). \tag{21}$$

On defining the non-dimensional time mean flows θ' and F respectively in the laboratory and wave frame as

$$\theta' = \frac{Q'}{cd_1}, \quad F = \frac{q}{cd_1}. \tag{22}$$

Thus Eq. (21) reduces to

$$\theta' = F + 1 + d, \tag{23}$$

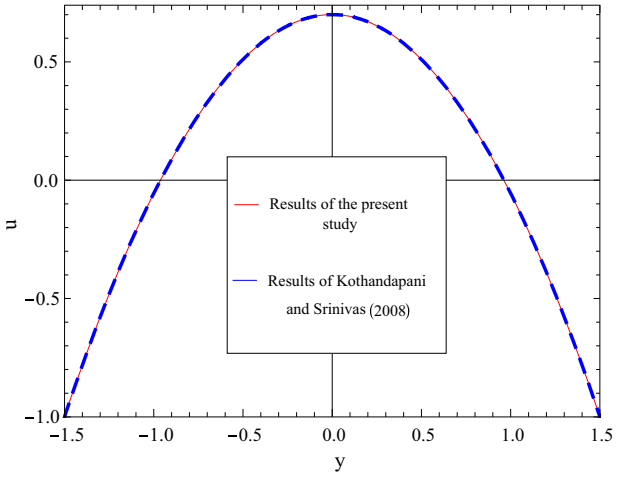

Fig. 2 Comparison of axial velocity distribution for $M = 0.0$, $Gr = 0.0$, $\alpha = 0.0$ and $\beta_1 = 0.0$ with the numerical results of Kothandapani and Srinivas [38].

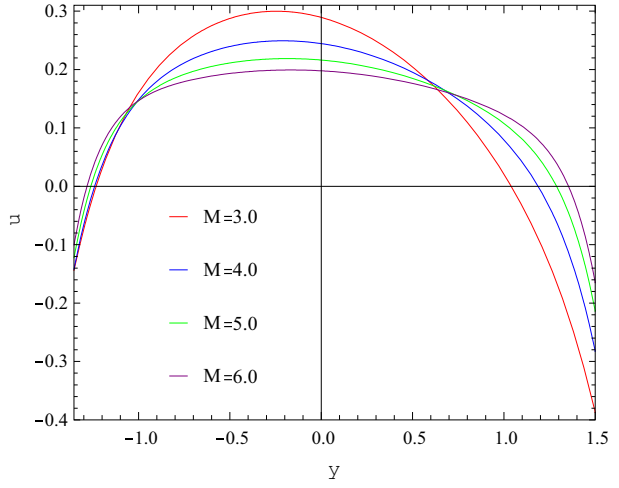

Fig. 3 Axial velocity profiles for different values of M with $a = b = 0.5$, $d = 1.0$, $\beta = 0.5$, $\beta_1 = 0.5$, $\theta' = 2.4$, $Gr = 5.0$, $\alpha = 0.05$, $\gamma = 0.1$ and $\phi = \pi/4$).

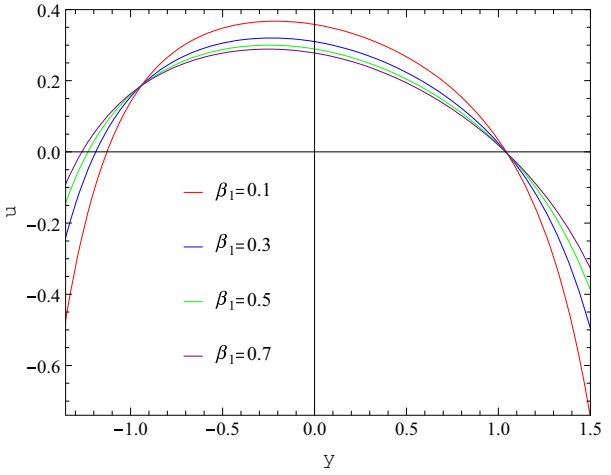

Fig. 4 Axial velocity profiles for different values of β_1 when $a = b = 0.5$, $d = 1.0$, $\beta = 0.5$, $M = 4.0$, $\theta' = 2.4$, $Gr = 5.0$, $\alpha = 0.05$, $\gamma = 0.1$ and $\phi = \pi/4$.

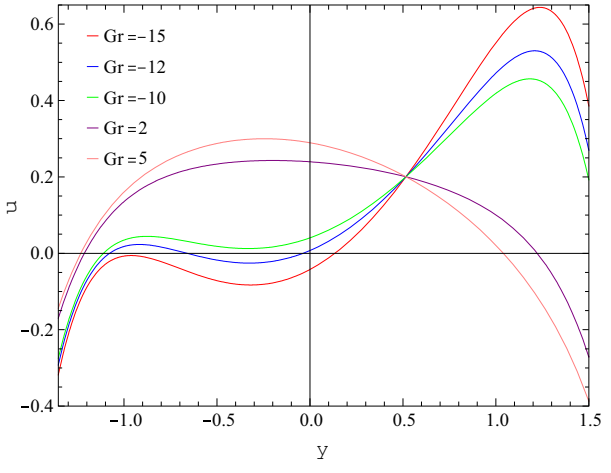

Fig. 5 Axial velocity profiles for different values of Gr when $a = b = 0.5, d = 1.0$, $\beta = 0.5$, $\beta_1 = 0.5$, $\theta' = 2.4$, $M = 4.0$, $\alpha = 0.05$, $\gamma = 0.1$ and $\phi = \pi/4$.

where $d = \frac{d_2}{d_1}$ and

$$F = \int_{h_2}^{h_1} \frac{\partial \psi}{\partial y} dy = \psi(h_1) - \psi(h_2). \tag{24}$$

The non-dimensional form of the equations channel walls gives rise to

$$h_1 = \frac{h_1'}{d_1} = 1 + a\cos(2\pi x),$$
$$\text{and} \qquad h_2 = \frac{h_2'}{d_1} = -d - b\cos(2\pi x + \phi), \tag{25}$$

in which

$$a = \frac{a_1}{d_1} \quad \text{and} \quad b = \frac{a_2}{d_1}. \tag{26}$$

Also a, b and ϕ satisfy the following relation

$$a^2 + b^2 + 2ab\cos\phi \leqslant (1+d)^2. \tag{27}$$

The dimensionless slip condition in the wave frame is

$$\psi = \frac{F}{2},\ \frac{\partial \psi}{\partial y} + \beta_1 \frac{\partial^2 \psi}{\partial y^2} = -1 \ \text{ and } \ \theta + \gamma \frac{\partial \theta}{\partial y} = 0 \ \text{ at } y = h_1, \tag{28}$$

$$\psi = -\frac{F}{2},\ \frac{\partial \psi}{\partial y} - \beta_1 \frac{\partial^2 \psi}{\partial y^2} = -1 \ \text{ and } \ \theta - \gamma \frac{\partial \theta}{\partial y} = 0 \ \text{ at } y = h_2, \tag{29}$$

in which $\beta_1 \left(= \frac{\beta_1'}{d_1}\right)$ and $\gamma \left(= \frac{\gamma'}{d_1}\right)$ are the non-dimensional velocity and thermal slip parameters.

As mentioned in previous communications [39,40], although the viscosity μ depends on y and θ, the viscosity μ

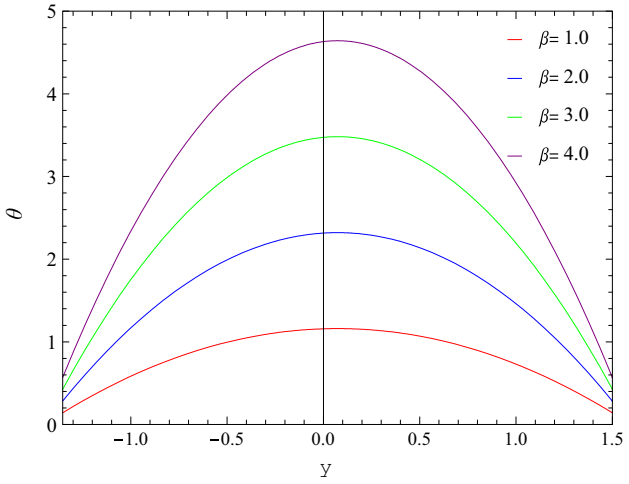

Fig. 6 Temperature distribution for different values of β with $a = b = 0.5$, $d = 1.0$, $Gr = 5.0$, $\beta_1 = 0.5$, $\theta' = 2.4$, $M = 4.0$, $\alpha = 0.05$, $\gamma = 0.1$ and $\phi = \pi/4$.

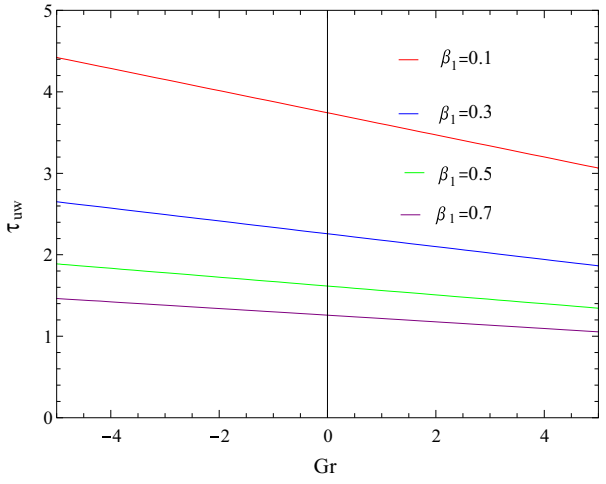

Fig. 8 Variation of shear stress at the upper wall with Gr for different values of β_1 with $a = b = 0.5$, $d = 1.0$, $\beta = 0.5$, $\theta' = 2.4$, $M = 4.0$, $\alpha = 0.05$, $\gamma = 0.1$ and $\phi = \pi/4$.

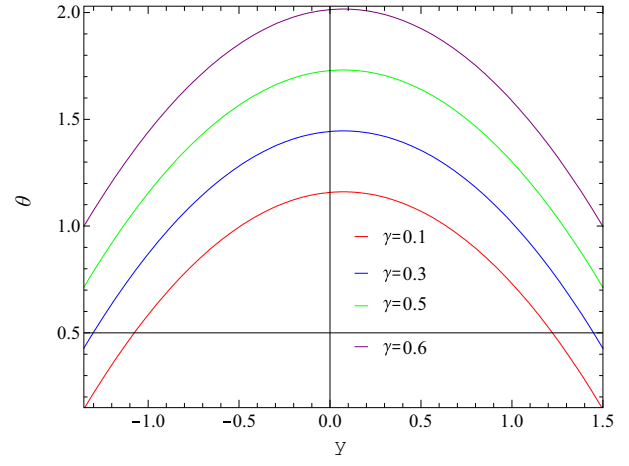

Fig. 7 Temperature distribution for different values of γ with $a = b = 0.5$, $d = 1.0$, $Gr = 5.0$, $\beta_1 = 0.5$, $\theta' = 2.4$, $M = 4.0$, $\alpha = 0.05$, $\beta = 0.5$ and $\phi = \pi/4$.

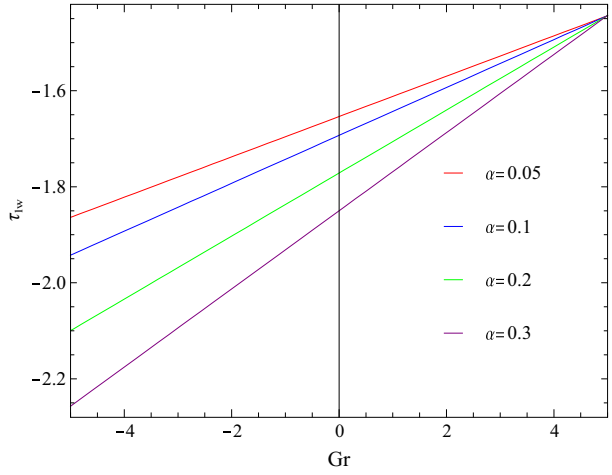

Fig. 9 Variation of shear stress at the lower wall with Gr for different values of α with $a = b = 0.5$, $d = 1.0$, $\beta = 0.5$, $\theta' = 2.4$, $M = 4.0$, $\beta_1 = 0.5$, $\gamma = 0.1$ and $\phi = \pi/4$.

can be taken as a function of y only. For our analysis, we consider the following form of μ

$$\mu(y) = 1 - \alpha y \quad \text{for } \alpha \ll 1, \tag{30}$$

where α is Reynolds model viscosity parameter. The choice of μ is justified physiologically because normal human being or animal of similar size takes $1-2L$ of the fluid everyday. Also $6-7L$ of the fluid is recurred by a small intestine as secretions from salivary glands, stomach, pancreas, liver and small intestine itself.

4. Perturbation analysis

The Reynolds model viscosity parameter α is considered to be very small. In order to solve Eq. (14) with the help of boundary conditions (28) and (29), we consider the perturbation expansion by writing

$$f = f_0 + \alpha f_1 + \alpha^2 f_2 + \cdots, \tag{31}$$

where f can replace ψ , F or p.

Now differentiating Eq. (14) with respect to y and substituting Eq. (31) and collecting the co-efficients of like power of α, one gets the zeroth-order equation as

$$\frac{\partial^4 \psi_0}{\partial y^4} - M^2 \frac{\partial^2 \psi_0}{\partial y^2} + Gr \frac{\partial \theta}{\partial y} = 0 \tag{32}$$

along with the corresponding boundary conditions

$$\psi_0 = \frac{F_0}{2}, \quad \frac{\partial \psi_0}{\partial y} + \beta_1 \frac{\partial^2 \psi_0}{\partial y^2} = -1 \quad \text{at } y = h_1 \tag{33}$$

and

$$\psi_0 = -\frac{F_0}{2}, \quad \frac{\partial \psi_0}{\partial y} - \beta_1 \frac{\partial^2 \psi_0}{\partial y^2} = -1 \quad \text{at } y = h_2. \tag{34}$$

The first-order perturbation equation is found in the form

$$\frac{\partial^4 \psi_1}{\partial y^4} - y \frac{\partial^4 \psi_0}{\partial y^4} - 2 \frac{\partial^3 \psi_0}{\partial y^3} - M^2 \frac{\partial^2 \psi_1}{\partial y^2} = 0. \tag{35}$$

The corresponding boundary conditions are

$$\psi_1 = \frac{F_1}{2}, \quad \frac{\partial \psi_1}{\partial y} + \beta_1 \frac{\partial^2 \psi_1}{\partial y^2} = 0 \quad \text{at } y = h_1 \tag{36}$$

and

$$\psi_1 = -\frac{F_1}{2}, \quad \frac{\partial \psi_1}{\partial y} - \beta_1 \frac{\partial^2 \psi_1}{\partial y^2} = 0 \quad \text{at } y = h_2. \tag{37}$$

5. Solution of the problem

The temperature Eq. (16) satisfy the boundary conditions (28) and (29) yields

$$\theta = -\frac{\beta y^2}{2} + c_1 y + c_2, \tag{38}$$

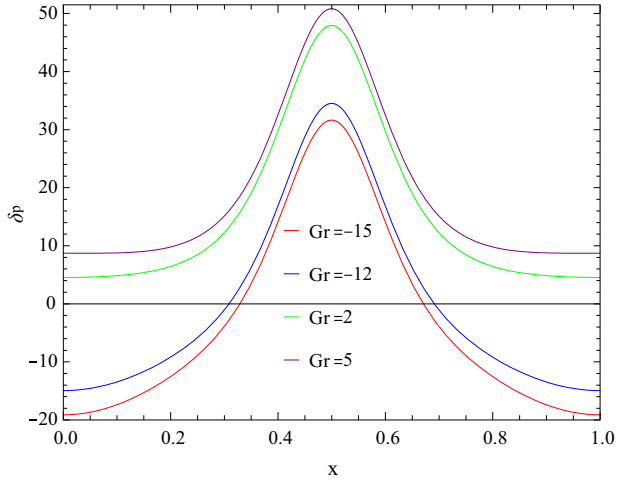

Fig. 10 Variation of $\frac{dp}{dx}$ with x for different values of Gr when $a = b = 0.5$, $d = 1.0$, $\beta = 0.5$, $\beta_1 = 0.5$, $\theta' = 2.4$, $M = 4.0$, $\alpha = 0.05$, $\gamma = 0.1$ and $\phi = \pi/4$.

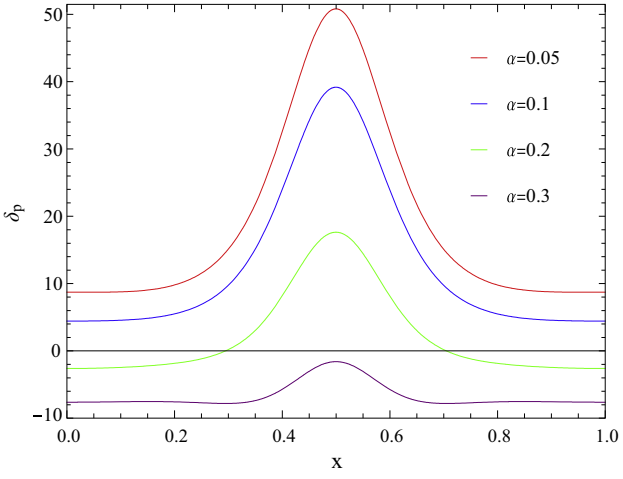

Fig. 11 Variation of $\frac{dp}{dx}$ with x for different values of α when $a = b = 0.5$, $d = 1.0$, $\beta = 0.5$, $\beta_1 = 0.5$, $\theta' = 2.4$, $M = 4.0$, $Gr = 5.0$, $\gamma = 0.1$ and $\phi = \pi/4$.

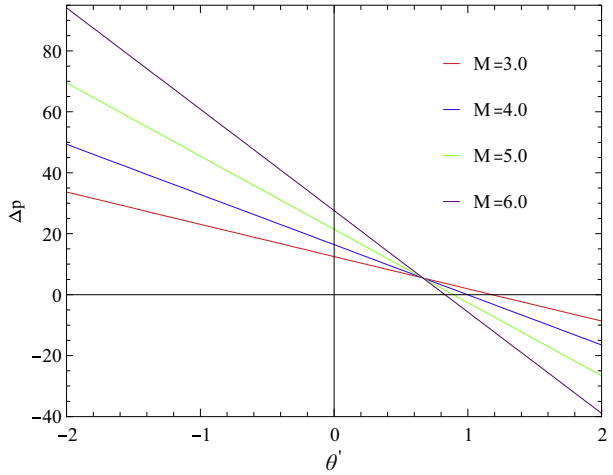

Fig. 12 Variation of Δp with θ' for different values of M when $a = b = 0.5$, $d = 1.0$, $\beta = 0.5$, $\beta_1 = 0.5$, $\alpha = 0.05$, $Gr = 5.0$, $\gamma = 0.1$ and $\phi = \pi/4$.

where the integrating constants $c_i,\ i = 1,\ 2$ obtained by using boundary conditions (28) and (29) are given in Appendix A.

5.1. Case I ($M = 0$)

With the help of Eq. (38) and using the boundary conditions (33) and (34), we can solve Eq. (32) by considering $M = 0$. The analytical expression for ψ_0 may be written as in following form

$$\psi_0 = c_3 + c_4 y + c_5 \frac{y^2}{2} + c_6 \frac{y^3}{6} + \frac{y^4}{24}\left(\frac{\beta y}{5} - c_1\right) Gr, \tag{39}$$

where the integrating constants $c_i,\ i = 3, \ldots, 6$ are given in Appendix A.

Now using the above expression of ψ_0, we can obtain the solution of ψ_1 by solving Eq. (35) under the boundary conditions (36) and (37) (when $M = 0$) as

$$\psi_1 = c_7 + c_8 y + c_9 \frac{y^2}{2} + c_{10} \frac{y^3}{6} + c_6 \frac{y^4}{12} - c_1 \frac{y^5}{60} Gr + \beta \frac{y^6}{240} Gr, \tag{40}$$

where the integrating constants $c_i,\ i = 7, \ldots, 10$ are given in Appendix A.

5.2. Case II ($M \neq 0$)

Using the expression of θ which is given in Eq. (38), we can solve Eq. (32) under the boundary conditions (33) and (34) as

$$\psi_0 = A_1 + A_2 y + A_3 e^{My} + A_4 e^{-My} - \frac{Gry^2}{6M^3}(\beta My - 3c_1 M + 3\beta). \tag{41}$$

Using the solution given in Eq. (41), we can solve the Eq. (35) with the help of (36) and (37) as

$$\psi_1 = A_5 + A_6 y + A_7 e^{My} + A_8 e^{-My} + \frac{A_3}{4} M e^{My} y(y-5) - \frac{A_4 M}{4} e^{-My} y(y+5) + \frac{A_3 e^{My}}{2} y^2 + A_4 e^{-My} 2y^2 - \frac{Gr\beta y^2}{M^4}, \tag{42}$$

where the integrating constants $A_i,\ i = 1, \ldots, 8$ are given in Appendix A.

The axial pressure can be written in the form

$$\frac{dp}{dx} = -\alpha \frac{\partial^2 \psi}{\partial y^2} + (1 - \alpha y) \frac{\partial^3 \psi}{\partial y^3} - M^2 \left(\frac{\partial \psi}{\partial y} + 1\right) + Gr\theta. \tag{43}$$

The non-dimensional expression for the pressure rise per wavelength Δp is given by

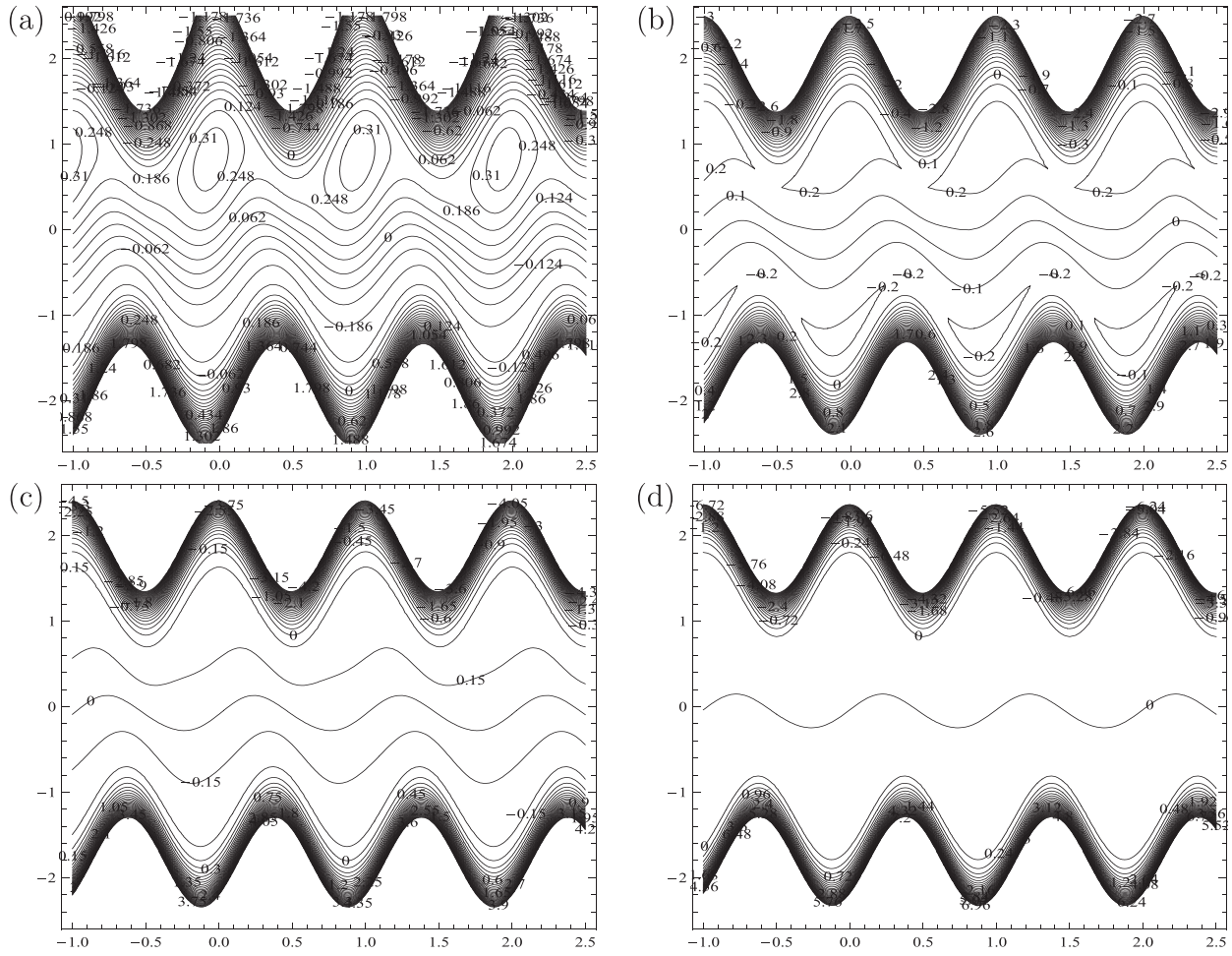

Fig. 13 Streamline patterns for (a) $M = 3$, (b) $M = 4$, (c) $M = 5$ and (d) $M = 6$ with $a = b = 0.5$, $d = 1.0$, $\beta = 0.5$, $\beta_1 = 0.5$, $\theta' = 2.4$, $Gr = 5.0$, $\alpha = 0.05$, $\gamma = 0.1$ and $\phi = \pi/4$.

$$\Delta p = \int_0^1 \left(\frac{dp}{dx}\right) dx. \tag{44}$$

6. Results and discussion

This section is divided into six subsections. In Section 6.1, we give the comparison of our results with the previous results. In Sections 6.2–6.4, the effects of various parameters on velocity profiles, temperature distribution and wall shear stress are investigated. The pumping characteristics are discussed in Section 6.5 and in Section 6.6 we have illustrated the trapping phenomena.

6.1. Model validation

Fig. 2 gives the comparison between the results obtained in the present study and the results of Kothandapani and Srinivas [38]. For the purpose of comparison, both the studies have been naturally brought to the same platform, by considering equal parametric values in the absence of magnetic field as well as by disregarding the slip effects for the present study. For comparison, we neglected the heat transfer effect by setting $Gr = 0$ and assumed that the viscosity is constant while taking $\alpha = 0$. On the other hand, in the analytical solution of the velocity profiles presented by Kothandapani and Srinivas [38], we considered a large value of permeability parameter with zero inclination angle. One may observe from this figure that the results of the present study are in good agreement with those of the previous study.

6.2. Velocity distribution

Figs. 3–5 focus on the axial velocity u for different values of Hartman number (magnetic parameter), velocity-slip parameter and Grashof number respectively. Fig. 3 reveals that at the near of the arterial walls, axial velocity increases with increasing Hartman number, whereas the reversed trend is observed in the central region of the artery in the case of cooling of the arterial walls i.e, when $Gr > 0$. This observation agrees with the theory because with the increase in Hartman number, the Lorentz force increases. It is well known that Lorentz force opposes the flow. This implies that if we increase the strength of magnetic field, the flow of blood will be impeded. From Fig. 4, we observed that for any values of velocity-slip parameter, the axial velocity vanishes at two different points. These points are the points of inflexion. This result indicates that the flow reversal occurs at these points. It is also noted that the axial velocity decreases in the central region and increases near the channel walls for increasing velocity slip parameter β_1.

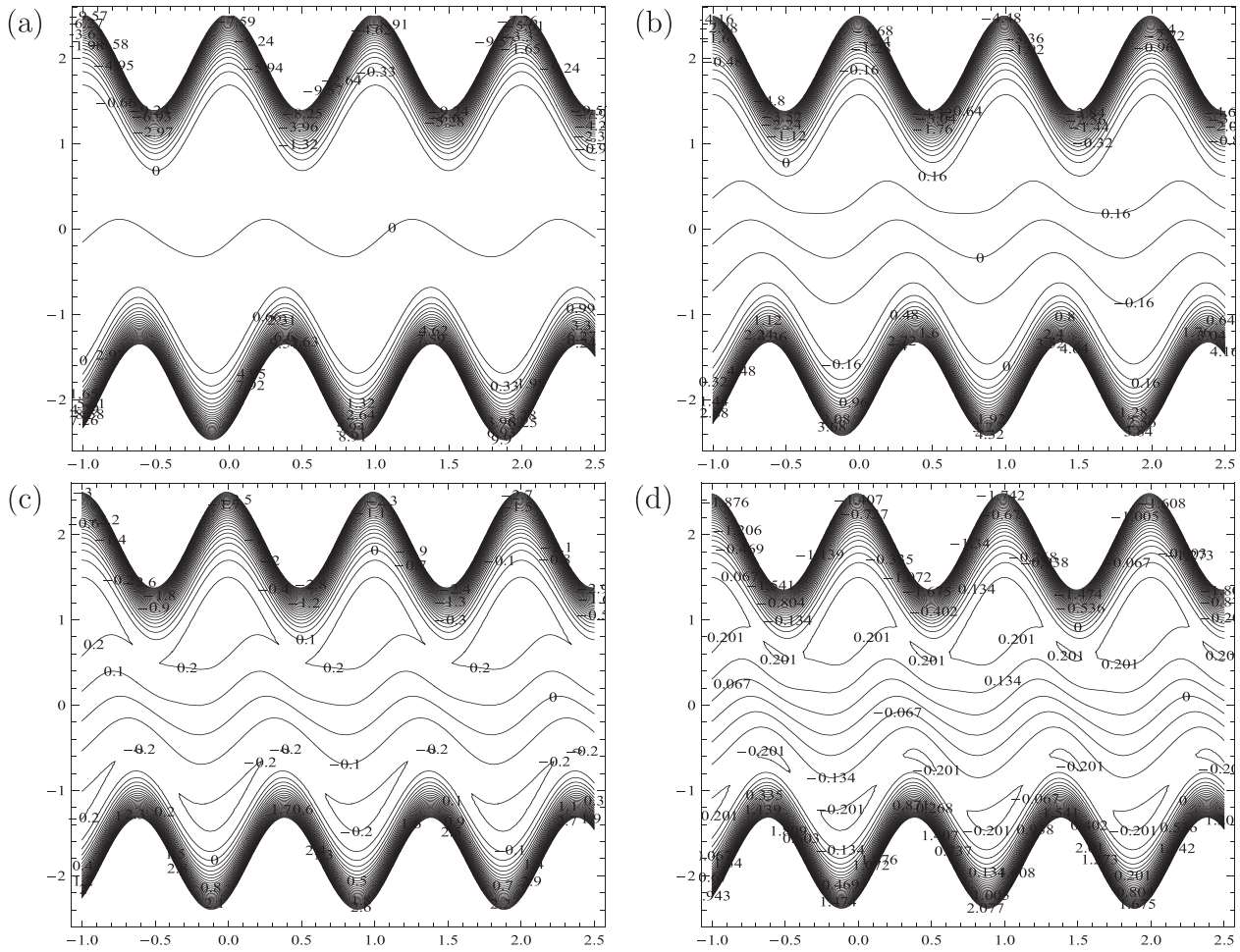

Fig. 14 Streamline patterns for (a) $\beta_1 = 0.1$, (b) $\beta_1 = 0.3$, (c) $\beta_1 = 0.5$ and (d) $\beta_1 = 0.7$ with $a = b = 0.5$, $d = 1.0$, $\beta = 0.5$, $M = 4.0$, $\theta' = 2.4$, $Gr = 5.0$, $\alpha = 0.05$, $\gamma = 0.1$ and $\phi = \pi/4$.

One can have an idea of velocity distribution for both cases i.e, the cooling of the arterial walls ($Gr > 0$) and heating of the arterial walls ($Gr < 0$) from Fig. 5. It may be noted that in the case of cooling, velocity increases with increasing Grashof number up to a certain height of the artery, beyond which a reverse trend is observed, whereas in the case of heating, velocity decreases up to a certain distance from the lower wall of the artery and after that velocity decreases with increasing Grashof number. It is also seen from this figure that for $Gr = -12$, velocity vanishes at three different points whereas for other values of Gr, velocity vanishes twice.

6.3. Temperature distribution

Figs. 6 and 7 give some characteristic temperature profiles for different values of heat source parameter and thermal-slip/temperature jump factor respectively. Fig. 6 emphasizes that as heat generates during blood flow in arterioles, there is a significant rise in thickness of boundary layer. Thereby the temperature of the boundary layer enhanced by appreciable extend. It is also noticed from this figure that the maximum value of temperature attains in the central region of the channel. Fig. 7 indicates that temperature increases as the temperature jump factor increases. It may also be noted from this figure that for any values of γ, temperature increases with the height of the channel and after attaining its maximum, it decreases.

6.4. Wall shear stress

It is widely accepted fact that the wall shear stress plays an important role in the development of arteriole disease. Hence it is important to study the effects of the parameters β_1, α and Gr on the wall shear stress. Fig. 8 depicts the variation of shear stress at the upper wall of an artery for different values of velocity-slip parameter in the case of heating as well as cooling of the arterial walls. The figure shows that for both cases, shear stress decreases at the upper wall of an artery with the increasing values of velocity-slip parameter. It is also observed that in the case of heating of the walls ($Gr < 0$), shear stress at the upper wall increases with increasing Gr, whereas the reversed trend is observed in the case of cooling of the walls. Fig. 9 reveals that the shear stress at the lower wall decreases as Reynolds model viscosity parameter (α) increases.

6.5. Pumping characteristics

This subsection describes the influence of various emerging parameters involving in our problem on the axial pressure

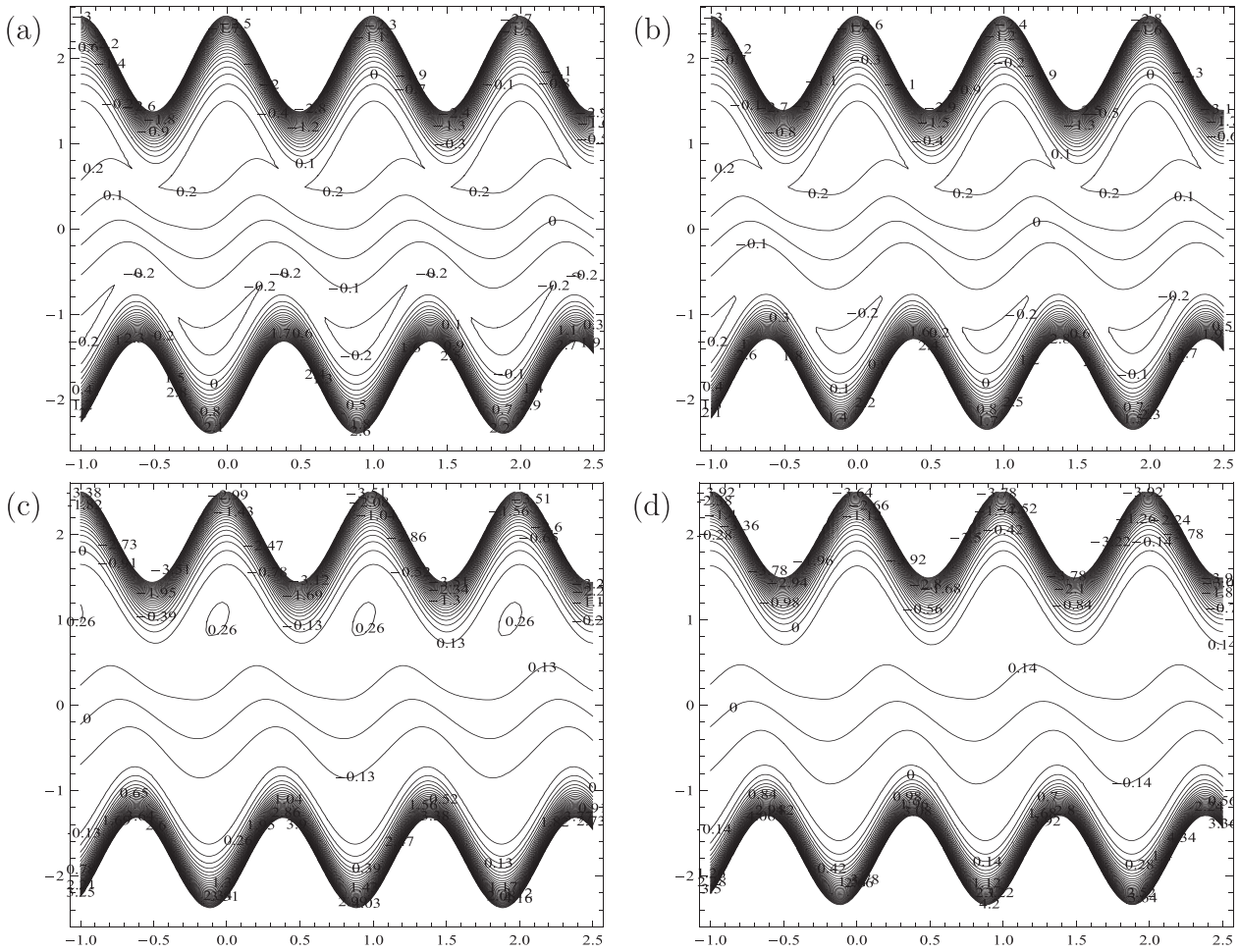

Fig. 15 Streamline patterns for (a) $\alpha = 0.05$, (b) $\alpha = 0.1$, (c) $\alpha = 0.2$ and (d) $\alpha = 0.3$ with $a = b = 0.5$, $d = 1.0$, $\beta = 0.5$, $\beta_1 = 0.5$, $\theta' = 2.4$, $Gr = 5.0$, $M = 4$, $\gamma = 0.1$ and $\phi = \pi/4$.

gradient $\frac{dp}{dx}$ and the pressure rise per wavelength Δp. The effect of these parameters is shown by Figs. 10–12. Figs. 10 and 11 illustrate that in the wider part of an artery, $0 \leqslant x \leqslant 0.35$ and $0.65 \leqslant x \leqslant 1$, the pressure gradient is relatively small, that is, the flow can easily pass without imposition of large pressure gradient. Where, in the narrow part of artery, $0.35 \leqslant x \leqslant 0.65$, a much larger pressure gradient is required to maintain the same flux to pass it, especially for the narrowest position $x = 0.5$. This is in well agreement with the physical situation. Also from these two figures we observe that the effect of Grashof number and Reynolds model viscosity parameter on the pressure gradient for fixed value of other parameters. Fig. 10 shows that the amplitude of pressure gradient increases with increasing Gr in the case of cooling of the arterial walls ($Gr > 0$), whereas a reverse trend is observed in the case of heating of the arterial walls ($Gr < 0$). Fig. 11 reveals that in case of cooling of the walls, the amplitude of pressure gradient decreases with increasing α. Fig. 12 illustrates the change of pressure rise Δp versus the time average mean flow rate θ' for different values of Hartman number M (3, 4, 5, 6). One may observe from this figure that in the range of values of pressure gradient examined in the present study, the volumetric flow rate increases with the increase in the magnetic parameter in the pumping region when $\Delta p > 8$ and decreases in the pumping region when $\Delta p < 8$ and free pumping region ($\Delta p = 0$) as well as in the co-pumping region ($\Delta p < 0$). It is also seen from this figure that there is an inversely linear relation between Δp and θ', i.e. the pressure rise decreases with increasing flow rate.

6.6. Trapping phenomena

The formation of an internally circulating bolus of the fluid by closed streamline is called trapping and this trapped bolus pulled ahead along with the peristaltic wave. Since this bolus appears to be trapped by the wave, the bolus moves with the same speed as that of the wave. Fig. 13 illustrates the streamline patterns and trapping for different values of the Hartman number M corresponding to $\alpha = 0.05,\ Gr = 5.0,\ \beta_1 = 0.5$ and $\theta' = 2.4$. It is observed that the volume of the bolus decreases with increase of M and slowly disappears for the large value of M, where the fluid moves as a bulk. One may note from these figures that only for $M = 4$, bolus appears near the lower wall of artery. Formation of trapping zone and streamline patterns is depicted in Fig. 14 for different values of velocity-slip parameter β_1. These figures reveal that with a reduction in β_1, the trapping zone decreases and it disappears completely when β_1 attains the value 0.3. Plots showing the effect of the Reynolds model viscosity parameter on trapping are presented in Fig. 15. One can observe that size of the trapped bolus

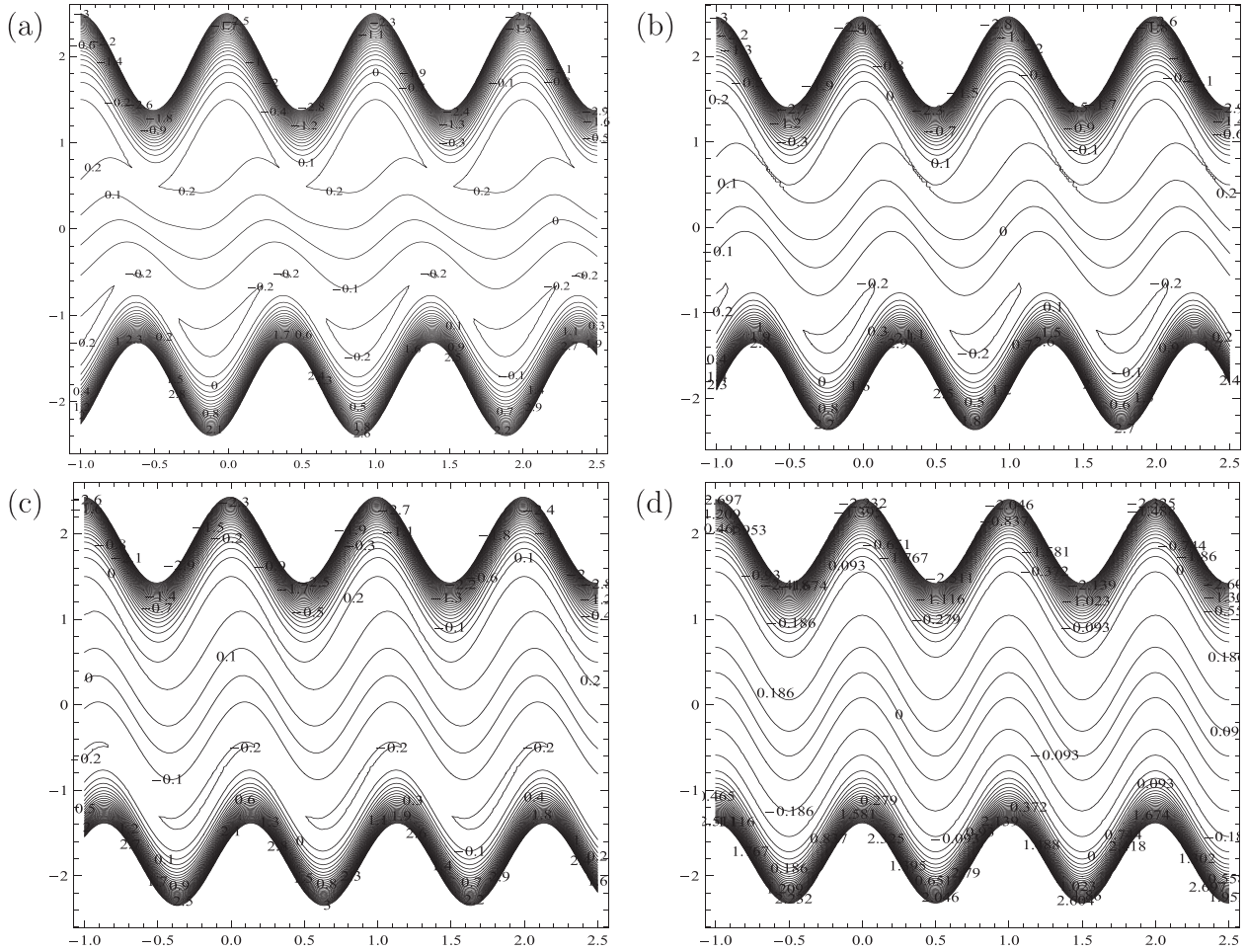

Fig. 16 Streamline patterns for (a) $\phi = \frac{\pi}{4}$, (b) $\phi = \frac{\pi}{2}$, (c) $\phi = \frac{3\pi}{4}$ and (d) $\phi = \pi$ with $a = b = 0.5,\ d = 1.0,\ \beta = 0.5,\ \beta_1 = 0.5,\ \theta' = 2.4,\ Gr = 5.0,\ \alpha = 0.05,\ \gamma = 0.1$ and $M = 4$.

decreases with increase in α and vanish when $\alpha = 0.3$. The effects of the phase difference ϕ on the trapping can be seen through Fig. 16. It is found that for small values of ϕ, trapping exists and the size of the trapped bolus is large and decreases in size when ϕ increases and vanishes for $\phi = \pi$.

7. Concluding remarks

A study is made in order to explain the peristaltic transport of a MHD flow of blood with variable viscosity and heat transfer in an asymmetric arteriole in the presence velocity-slip and temperature jump. The governing two-dimensional equations have been modeled and then simplified using long wave length approximation. Closed form analytic solutions are constructed for axial velocity, temperature and stream function. The effects of various emerging parameters on the axial velocity, temperature, axial pressure gradient, pressure rise over a wavelength, wall shear stresses and stream line flow patterns are seen with the help of graphs. From the presented analysis the following conclusions can be drawn:

- The velocity of blood can be controlled by regulating the magnetic field strength. This result is very much important at the time of surgery.
- As heat generation increases, the thermal boundary layer thickness increases by an appreciable extent. This result is very much important in the case of electromagnetic hyperthermia treatment. Because the main objective of electromagnetic hyperthermia is to rise the cancerous tissues above 42 °C.
- Wall shear stress at the upper wall increases with velocity-slip parameter, whereas the wall shear stress at the lower wall decreases with increasing α in the case of cooling of the arterial walls.
- It is possible to enhance the pressure rise Δp as well as the peristaltic pumping performance by increasing the intensity of magnetic parameter.
- An increase in the Reynolds model viscosity parameter reduces the size of trapped bolus, and ultimately vanishes when the viscosity parameter is large.

Acknowledgments

The authors wish to convey their sincere thanks to all the esteemed reviewers for their comments and suggestions based upon which the present version of the manuscript has been revised. The authors are grateful to the Department of Science and Technology (DST), Govt. of India, New Delhi for financial support of this investigation.

Appendix A. The expressions that appear in Section 5 are listed as follows

$$c_1 = \frac{1}{2}\beta(h_1+h_2), \quad c_2 = \frac{1}{2}\beta h_2^2 - \beta\gamma h_2 + c_1(\gamma - h_2),$$

$$c_3 = \frac{F_0}{2} - c_4 h_1 - \frac{1}{2}c_5 h_1^2 - \frac{1}{6}c_6 h_1^3 - \frac{1}{24}Gr h_1^4\left(\frac{1}{5}\beta h_1 - c_1\right),$$

$$c_4 = -1 - E_1 - c_5(h_1+\beta_1) - c_6 h_1(\beta_1 + \frac{1}{2}h_1),$$

$$c_5 = \frac{1}{E_6}(E_8 - E_7 c_6), \quad c_6 = \frac{E_5E_6 - E_8E_3}{E_4E_6 - E_3E_7},$$

$$c_7 = \frac{F_1}{2} - c_8 h_1 - \frac{1}{2}c_9 h_1^2 - \frac{1}{6}c_{10}h_1^3 - R_1,$$
$$c_8 = -R_5 - R_3 c_9 - R_4 c_{10},$$

$$c_9 = \frac{1}{R_{12}}(R_{14} - c_{10}R_{13}), \quad c_{10} = \frac{R_{11}R_{12} - R_{14}R_9}{R_{10}R_{12} - R_{13}R_9},$$

$$E_1 = \frac{Gr h_1^2}{2}\left[\frac{1}{3}h_1\left(\frac{1}{4}\beta h_1 - c_1\right) + \beta_1\left(\frac{1}{3}\beta h_1 - c_1\right)\right],$$

$$E_2 = \frac{Gr h_2^2}{2}\left[\frac{1}{3}h_2\left(\frac{1}{4}\beta h_2 - c_1\right) - \beta_1\left(\frac{1}{3}\beta h_2 - c_1\right)\right],$$

$$E_3 = h_1 - h_2 + 2\beta_1, \quad E_4 = (h_1+h_2)\left[\frac{1}{2}(h_1-h_2) + \beta_1\right],$$
$$E_5 = E_2 - E_1,$$

$$E_6 = \frac{1}{2}(h_1-h_2)(h_2 - h_1 - 2\beta_1),$$
$$E_7 = (h_1-h_2)\left[h_1^2 + h_1h_2 + h_2^2 - h_1\left(\beta_1 + \frac{1}{2}h_1\right)\right],$$

$$E_8 = F_0 + (1+E_1)(h_1-h_2) - \frac{1}{24}Gr\left[\frac{1}{5}\beta(h_1^5 - h_2^5) - c_1(h_1^4 - h_2^4)\right],$$

$$R_1 = \frac{1}{12}c_6 h_1^4 - \frac{Gr}{60}c_1 h_1^5 + \frac{Gr}{240}\beta h_1^6,$$
$$R_2 = \frac{1}{12}c_6 h_2^4 - \frac{Gr}{60}c_1 h_2^5 + \frac{Gr}{240}\beta h_2^6,$$

$$R_3 = h_1 + \beta_1, \quad R_4 = h_1\left(\beta_1 + \frac{1}{2}h_1\right),$$
$$R_5 = c_6 h_1^2\left(\frac{1}{3}h_1 + \beta_1\right) - \frac{Gr}{3}c_1 h_1^3\left(\frac{1}{4}h_1 + \beta_1\right) + \frac{Gr}{8}\beta h_1^4\left(\frac{1}{5}h_1 + \beta_1\right),$$

$$R_6 = h_2 - \beta_1, \quad R_7 = h_1\left(-\beta_1 + \frac{1}{2}h_2\right),$$
$$R_8 = c_6 h_2^2\left(\frac{1}{3}h_2 - \beta_1\right) - \frac{Gr}{3}c_1 h_2^3\left(\frac{1}{4}h_2 - \beta_1\right) + \frac{Gr}{8}\beta h_2^4\left(\frac{1}{5}h_2 - \beta_1\right),$$

$$R_9 = R_3 - R_6, \quad R_{10} = R_4 - R_7, \quad R_{11} = R_8 - R_5,$$
$$R_{12} = \frac{1}{2}(h_1-h_2)(h_1+h_2-2R_3),$$

$$R_{13} = \frac{1}{6}(h_1-h_2)(h_1^2 + h_1h_2 + h_2^2 - 6R_4),$$
$$R_{14} = F_1 - R_1 + R_2 + R_5(h_1-h_2),$$

$$A_1 = \left[\frac{F_0}{2} - A_2h_1 - A_3e^{Mh_1} - A_4e^{-Mh_1} + \frac{Gr h_1^2}{6M^3}(\beta M h_1 - 3c_1M + 3\beta)\right],$$
$$A_2 = [J_3 - J_1A_3 - J_2A_4],$$

$$A_3 = \left[\frac{1}{J_{14}}(J_{16} - J_{15}A_4)\right], \quad A_4 = \left[\frac{J_{11}J_{16} - J_{13}J_{14}}{J_{11}J_{15} - J_{12}J_{14}}\right],$$
$$J_1 = \left(Me^{Mh_1} + \beta_1 M^2 e^{Mh_1}\right),$$

$$J_2 = \left(\beta_1 M^2 e^{-Mh_1} - Me^{-Mh_1}\right),$$
$$J_3 = \left[-1 + \frac{Gr}{3M^3}(h_1 + \beta_1)(\beta M h_1 - 3c_1 M + 3\beta) + \frac{Grh_1^2\beta}{6M^2} + \frac{2Grh_1\beta\beta_1}{3M^2}\right],$$

$$J_4 = \left(Me^{Mh_2} - \beta_1 M^2 e^{Mh_2}\right), \quad J_5 = \left(-\beta_1 M^2 e^{-Mh_2} - Me^{-Mh_2}\right),$$

$$J_6 = \left[-1 + \frac{Gr}{3M^3}(h_2 - \beta_1)(\beta M h_2 - 3c_1 M + 3\beta) + \frac{Grh_2^2\beta}{6M^2} - \frac{2Grh_2\beta\beta_1}{3M^2}\right],$$

$$J_7 = (h_1 - h_2), \quad J_8 = \left(e^{Mh_1} - e^{Mh_2}\right), \quad J_9 = \left(e^{-Mh_1} - e^{-Mh_2}\right),$$

$$J_{10} = \left(F_0 + \frac{Grh_1^2}{6M^3}(\beta M h_1 - 3c_1 M + 3\beta) - \frac{Grh_2^2}{6M^3}(\beta M h_2 - 3c_1 M + 3\beta)\right),$$
$$J_{11} = (J_1 - J_4),$$

$$J_{12} = (J_2 - J_5), \quad J_{13} = (J_3 - J_6), \quad J_{14} = (J_8 - J_1 J_7),$$
$$J_{15} = (J_9 - J_2 J_7), \quad J_{16} = (J_{10} - J_3 J_7),$$

$$A_5 = \left[\frac{F_1}{2} - A_6 h_1 - A_7 e^{Mh_1} - A_8 e^{-Mh_1} - G_1\right],$$
$$A_6 = \left[-G_8 - G_6 A_7 - G_7 A_8\right],$$

$$A_7 = \left[\frac{1}{G_{12}}(G_{14 - G_{13}A_8})\right], \quad A_8 = \left[\frac{G_{11}G_{12} - G_9 G_{14}}{G_{10}G_{12} - G_9 G_{13}}\right],$$

$$G_1 = \left[\frac{A_3}{4}Me^{Mh_1}h_1(h_1 - 5) - \frac{A_4 M}{4}e^{-Mh_1}h_1(h_1 + 5) + \frac{A_3 e^{Mh_1}h_1^2}{2} + \frac{A_4 e^{-Mh_1}h_1^2}{2} - \frac{Gr\beta h_1^2}{M^4}\right],$$

$$G_2 = \left[\frac{A_3}{4}Me^{Mh_2}h_2(h_2 - 5) - \frac{A_4 Me^{-Mh_2}h_2(h_2 + 5)}{4} + \frac{A_3 e^{Mh_2}h_2^2}{2} + \frac{A_4 e^{-Mh_2}h_2^2}{2} - \frac{Gr\beta h_2^2}{M^4}\right],$$

$$G_3 = \left[Me^{Mh_1} + \beta_1 M^2 e^{Mh_1}\right], \quad G_4 = \left[\beta_1 M^2 e^{-Mh_1} - Me^{-Mh_1}\right],$$

$$G_5 = \left[\frac{A_3}{4}e^{Mh_1}(h_1^2 - 5h_1)(M^2 + \beta_1 M^3) + \frac{A_3}{4}e^{Mh_1}(2h_1 - 5)(M + 2\beta_1 M^2) + \beta_1\frac{A_3}{2}Me^{Mh_1}\right.$$
$$+\frac{A_4}{4}M^2 e^{-Mh_1}(h_1^2 + 5h_1)(1 - \beta_1 M) + \frac{A_4}{4}Me^{-Mh_1}(2h_1 + 5)(\beta_1 M - 1)$$
$$+\frac{A_3}{2}Me^{Mh_1}(h_1^2) + A_3 e^{Mh_1} - \frac{A_4}{2}Me^{-Mh_1}(h_1^2) + A_4 e^{-Mh_1}h_1 - \frac{Gr\beta 2h_1}{M^4}$$
$$+\beta_1\left[\frac{A_4}{4}M^2 e^{-Mh_1}(2h_1 + 5) - \frac{A_4}{2}Me^{-Mh_1} + \frac{A_3}{2}M^2 e^{Mh_1}h_1^2 + A_3 Mh_1 e^{Mh_1}\right.$$
$$+A_3 Mh_1 e^{Mh_1} + A_3 e^{Mh_1} + \frac{A_4}{2}M^2 e^{-Mh_1}(h_1^2) - \frac{A_4 Me^{-Mh_1 2h_1}}{2}$$
$$\left.\left.+A_4 e^{-Mh_1} - A_4 e^{-Mh_1}h_1 M - \frac{2Gr\beta}{M^4}\right]\right],$$

$$G_6 = \left[Me^{Mh_2} - \beta_1 M^2 e^{Mh_2}\right], \quad G_7 = \left[-\beta_1 M^2 e^{-Mh_2} - Me^{-Mh_2}\right],$$

$$G_8 = \left[\frac{A_3}{4}e^{Mh_2}(h_2^2 - 5h_2)(M^2 - \beta_1 M^3) + \frac{A_3}{4}e^{Mh_2}(2h_2 - 5)(M - 2\beta_1 M^2)\right.$$
$$-\beta_1\frac{A_3}{2}Me^{Mh_2} + \frac{A_4}{4}M^2 e^{-Mh_2}(h_2^2 + 5h_2)(1 + \beta_1 M)$$
$$+\frac{A_4}{4}Me^{-Mh_2}(2h_2 + 5)(-\beta_1 M - 1) + \frac{A_3}{2}Me^{Mh_2}(h_2^2) + A_3 e^{Mh_2}$$
$$-\frac{A_4}{2}Me^{-Mh_2}(h_2^2) + A_4 e^{-Mh_2}h_2 - \frac{Gr\beta 2h_2}{M^4}$$
$$-\beta_1\left[\frac{A_4}{4}M^2 e^{-Mh_2}(2h_2 + 5) - \frac{A_4}{2}Me^{-Mh_2} + \frac{A_3}{2}M^2 e^{Mh_2}h_2^2 + A_3 Mh_2 e^{Mh_2}\right.$$
$$+A_3 Mh_2 e^{Mh_2} + A_3 e^{Mh_2} + \frac{A_4}{2}M^2 e^{-Mh_2}(h_2^2) - \frac{A_4 Me^{-Mh_2 2h_2}}{2} + A_4 e^{-Mh_2}$$
$$\left.\left.-A_4 e^{-Mh_2}h_2 M - \frac{2Gr\beta}{M^4}\right]\right],$$

$$G_9 = \left[e^{Mh_1} - e^{Mh_2} - (h_1 - h_2)G_3\right],$$
$$G_{10} = \left[e^{-Mh_1} - e^{-Mh_2} - (h_1 - h_2)G_4\right],$$

$$G_{11} = \left[F_1 - (G_1 - G_2) + (h_1 - h_2)G_5\right],$$
$$G_{12} = \left[(e^{Mh_1} - e^{Mh_2}) - (h_1 - h_2)G_6\right],$$

$$G_{13} = \left[(e^{-Mh_1} - e^{-Mh_2}) - (h_1 - h_2)G_7\right],$$
$$G_{14} = \left[F_1 - (G_1 - G_2) + (h_1 - h_2)G_8\right].$$

References

[1] Y.C. Fung, C.S. Yih, Peristaltic transport, J. Appl. Mech. 35 (1968) 669–675.
[2] A.H. Shapiro, M.Y. Jaffrin, S.L. Weinberg, Peristaltic pumping with long wavelengths at low Reynolds number, J. Fluid Mech. 37 (1969) 799–825.
[3] T.W. Latham, Fluid Motion in a Peristaltic Pump, M.Sc. thesis, Massachusetts Institute of Technology, Cambridge, 1966.
[4] A.C.T. Aarts, G. Ooms, Net flow of compressible viscous liquids induced by travelling waves in porous media, J. Eng. Math. 34 (1998) 435–450.
[5] K.DE. Vries, E.A. Lyons, G. Ballard, C.S. Levi, D.J. Lindsay, Contractions of the inner third of the myometrium, Am. J. Obstet. Gynecol. 162 (1990) 679–682.
[6] G. Taylor, Analysis of the swimming of microscopic organisms, Proc. R. Soc. Lond. A 209 (1951) 447–461.
[7] E.O. Carew, T.J. Pedley, An active membrane model for peristaltic pumping: Part I – Periodic activation waves in an infinite tube, J. Biomech. Eng. 119 (1997) 66–76.
[8] L.K. Antanovskii, H. Ramkissoon, Long-wave peristaltic transport of a compressible viscous fluid in a finite pipe subject to a time-dependent pressure drop, Fluid Dyn. Res. 19 (1997) 115–123.
[9] S. Nadeem, S. Akram, Peristaltic flow of a Williamson fluid in an asymmetric channel, Commun. Nonlinear Sci. Numer. Simulat. 15 (2010) 1705–1716.
[10] S. Maiti, J.C. Misra, Peristaltic flow of a fluid in a porous channel: a study having relevance to flow of bile within ducts in pathological state, Int. J. Eng. Sci. 49 (2011) 950–966.
[11] N.S. Akbar, A.W. Butt, Physiological transportation of Casson fluid in a plumb duct, Commun. Theor. Phys. 63 (2015) 347–352.
[12] A.EI. Hakeem, A.EI. Naby, A.E.M.EI. Misery, I.I.EI. Shamy, Effects of an endoscope and fluid with variable viscosity on peristaltic motion, Appl. Math Comput. 158 (2004) 497–511.
[13] A.M.EI. Misery, A.EI. Hakeem, A.EI. Naby, A.H.EI. Nagar, Effects of a fluid with variable viscosity and an endoscope on peristaltic motion, J. Phys. Soc. Jpn. 72 (2003) 89–93.

[14] E.F. Elshehawey, Z.M. Gharsseldien, Peristaltic transport of three-layered flow with variable viscosity, Appl. Math. Comput. 153 (2004) 417–432.
[15] B. Martin, Some analytical solutions for viscometric flows of power-law fluids with heat generation and temperature dependent viscosity, Int. J. Non-linear Mech. 2 (1967) 285–301.
[16] I.I.H. Chen, S. Sana, Analysis of an intensive magnetic field on blood flow: part 2, Electro. Biol. Medn. 4 (1985) 55–62.
[17] V.K. Sud, G.S. Sekhon, R.K. Mishra, Pumping action on blood flow by a magnetic field, Bull. Math. Biol. 39 (1977) 385–390.
[18] N.S. Akbar, Application of Eyring–Powell fluid model in peristalsis with nano particles, J. Comput. Theor. Nanosci. 12 (2015) 94–100.
[19] H.L. Agarwal, B. Anwaruddin, Peristaltic flow of blood in a branch, Ranchi Univ. Math. J. 15 (1984) 111–121.
[20] F.M. Abbasi, T. Hayat, A. Alsaedi, B. Ahmed, Soret and Dufour effects on peristaltic transport of MHD fluid with variable viscosity, Appl. Math. Inf. Sci. 8 (2014) 211–219.
[21] N.S. Akbar, Influence of magnetic field on peristaltic flow of a Casson fluid in an asymmetric channel: application in crude oil refinement, J. Magn. Magn. Mater. 378 (2015) 463–468.
[22] N.S. Akbar, Biological analysis of nano Prandtl fluid model in a diverging tube, J. Comput. Theor. Nanosci. 12 (2015) 105–112.
[23] N.S. Akbar, Heat transfer and carbon nano tubes analysis for the peristaltic flow in a diverging tube, Meccanica 50 (2015) 39–47.
[24] E. Lauga, H.A. Stone, Effective slip in pressure-driven Stokes flow, J. Fluid Mech. 489 (2003) 55–77.
[25] T. Hayat, Q. Hussain, N. Ali, Influence of partial slip on the peristaltic flow in a porous medium, Physica A 387 (2008) 3399–3409.
[26] T. Hayat, F.M. Abbasi, B. Ahmad, A. Alsaedi, Peristaltic transport of Carreau–Yasuda fluid in a curved channel with slip effects, PloS One 9 (2014) e95070.
[27] P. Brunn, The velocity slip of polar fluids, Rheol. Acta. 14 (1975) 1039–1054.
[28] Y. Nubar, Blood flow, slip and viscometry, Biophys. J. 13 (1973) 405–406.
[29] J.C. Misra, B.K. Kar, Momentum integral method for studying flow characteristics of blood through a stenosed vessel, Biorheology 26 (1989) 23–35.
[30] W.A. Ebert, E.M. Sparrow, Slip flow in rectangular and annular ducts, J. Fluids Eng. 87 (1965) 1018–1024.
[31] E.M. Sparrow, G.S. Beavers, L.Y. Hung, Channel and tube flows with surface mass transfer and velocity slip, Phys. Fluids 14 (1971) 1312–1319.
[32] C.Y. Wang, Flow due to a stretching boundary with partial slip – an exact solution of the Navier–Stokes equations, Chem. Eng. Sci. 57 (2002) 3745–3747.
[33] F.M. Abbasi, T. Hayat, B. Ahmad, G.Q. Chen, Slip effects on mixed convective peristaltic transport of copper–water nanofluid in an inclined channel, PloS One 9 (2014) e105440.
[34] T. Hayat, F.M. Abbasi, M. Al-Yami, S. Monaquel, Slip and Joule heating effects in mixed convection peristaltic transport of nanofluid with Soret and Dufour effects, J. Mol. Liquid 194 (2014) 93–99.
[35] A. Ogulu, A.R. Bestman, Blood flow in a curved pipe with radiative heat transfer, Acta. Phys. Hung. 74 (1994) 189–201.
[36] K. Vajravelu, G. Radhakrishnamacharya, V. Radhakrishnamurty, Peristaltic flow and heat transfer in a vertical porous annulus with long wave approximation, Int. J. Non Linear Mech. 42 (2007) 754–759.
[37] S. Srinivas, M. Kothandapani, Peristaltic transport in an asymmetric channel with heat transfer – a note, Int. Commun. Heat Mass Trans. 35 (2008) 514–522.
[38] M. Kothandapani, S. Srinivas, Non-linear peristaltic transport of a Newtonian fluid in an inclined asymmetric channel through a porus medium, Phys. Lett. A 372 (2008) 1265–1276.
[39] A.M.EI. Misery, A.EI. Hakeem, A.EI. Naby, A.H.EI. Nagar, Effects of a fluid with variable viscosity and an Endoscope on peristaltic motion, J. Phys. Soc. Jpn. 72 (2003) 89–93.
[40] A.EI. Hakeem, A.EI. Naby, A.E.M.EI. Misery, I.I.EI. Shamy, Hydromagnetic flow of fluid with variable viscosity in a uniform tube with peristalsis, J. Phys. A: Math. Gen. 36 (2003) 8535–8547.